TECTONICS, VOL. 8, NO. 3, PAGES 469-482, JUNE 1989

ORIGIN OF REGIONAL, ROOTED LOW-ANGLE NORMAL FAULTS: A MECHANICAL MODEL AND ITS TECTONIC IMPLICATIONS

An Yin[1]

Department of Geological Sciences,
University of Southern California,
Los Angeles

Abstract. Rooted listric low-angle normal faults ($< 20^0$) of regional extent have been recognized widely in the past few years in the North American Cordillera and elsewhere. The low-angle geometry of these crustal-scale normal faults conflicts with Anderson's [1942] classic theory of faulting. In that theory the orientations of principal stresses are assumed to be vertical and horizontal; the predicted dip angle of normal faults is about 60^0 rather than 20^0 or less. Recent geological and geophysical studies in the mid-Tertiary extensional terrane of southeastern California and western Arizona suggest that thick mylonitic gneisses in the lower plates of low-angle detachment faults may represent unidirectionally sheared laminar flow in and below the midcrust. Directed ductile flow, possibly related to the gravitational spreading of thickened lower crust, may induce a shearing traction on the horizontal or subhorizontal base of the brittle upper crust. Thus the orientations of the principal stresses can no longer be vertical and horizontal at this interface. A simple elastic model incorporates the effect of basal shearing due to gravitational spreading on stress distributions in an elastic upper crust. This model shows that parallel belts of compression and extension can be produced if a shearing traction acting on the base of the elastic upper crust is considered. In particular, appropriate stress conditions for the formation of regional low-angle normal faults ($< 20^0$) can be produced by the superposition of two stress fields: a basal shear stress field induced by the basal shear traction and a contractional stress field in which the horizontal deviatoric stress is compressional and the vertical gradient of the horizontal normal stress component is constant. This superposed stress field may represent a tectonic setting where a stress field with compressional deviatoric stress induced by plate subduction or convergence is superposed on a basal shear stress field induced by gravitational spreading of thickened lower crust. These results may explain both puzzling parallel belts of extension and compression and the occurrence of major low-angle normal faults in some orogenic systems.

[1]Now at Department of Earth and Space Sciences, University of California, Los Angeles.

Paper number 89TC00365.
0278-7407/89/89TC-00365$10.00

INTRODUCTION

Primary listric low-angle normal faults of regional extent, which root into the crust and maintain their low-angle geometry only a few kilometers below the surface, have been widely recognized in the North American Cordillera and elsewhere [e.g., Crittenden et al., 1980; Frost and Martin, 1982; Wernicke, 1981; Allmendinger et al., 1983; Burg et al., 1984; Green and Wernicke, 1986]. Primary listric low-angle normal faults are those that formed with low-angle geometry; their dip angles are usually less than 30^0 and can be as shallow as a few degrees [e.g., Burg et al., 1984]. These crustal-scale low-angle normal faults can be traced for several tens of kilometers in their dip direction [e.g., Davis et al., 1980; Allmendinger et al., 1983; John, 1987]. Their orientations are generally not controlled by preexisting structural [e.g., Wernicke et al., 1985] or fabric (e.g., foliations) anisotropies. Such faults have been interpreted as an important mode of deformation for intracontinental extension [Wernicke, 1985; Davis et al., 1986; Davis and Lister, 1988]. The shallow dip of crustal-scale normal faults (e.g., the spectacularly exposed Whipple detachment fault in southeastern California, [Davis et al., 1980]), however, conflicts with the prediction of classical fault mechanics proposed by Anderson [1942]. According to Anderson, the dip angle of normal faults associated with horizontal extension should be approximately 60^0 rather than 20^0 or less. The mechanical unlikelihood of low-angle normal faults in the context of Anderson's theory has become one of those faults' most perplexing and debated aspects.

A clue to resolving this mechanical paradox comes from recent geological and geophysical studies in the mid-

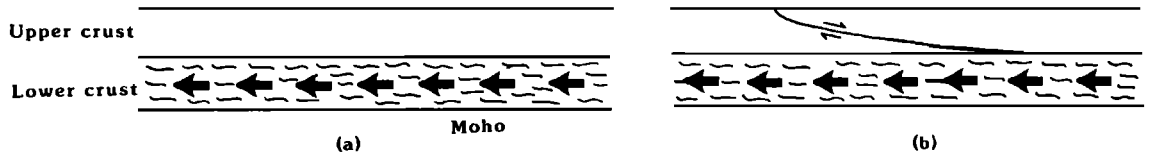

Fig. 1. Kinematic model for development of regional low-angle normal faults. (a) Ductile flow in lower crust produces basal shear traction. (b) Low-angle normal faults are initiated and cut across the brittle upper crust.

Tertiary extensional terrane of southeastern California and western Arizona. Unidirectionally sheared, thick (> 3.5 km) mylonitic gneisses formed during mid-Tertiary at depths >16 km [Wright, et al., 1986; Anderson, 1988] are kinematically compatible with the transport direction of major mid-Tertiary low-angle normal faults in the region [Davis et al., 1986]. Exposed mylonitic gneisses in the lower plate of the Whipple detachment fault have been correlated with subhorizontal reflectors of regional extent in and below the midcrust imaged by CALCRUST seismic reflection profiles [Frost and Okaya, 1987; Davis, 1988]. Such correlations imply that the midcrust and lower crust in the region was ductilely deformed and may represent a unidirectional shear zone [Frost and Okaya, 1987]. This interpretation is consistent with the inferred rheology of the continental lithosphere [e.g., Sibson, 1982; Chen and Molnar, 1983].

Directed ductile flow in and below the midcrust may be induced by gravitational spreading of thickened crust, a mechanism recently proposed for all or part of the Cenozoic extension in the North American Cordillera [Coney and Harms, 1984; Coney, 1987; Wernicke et al., 1987; Sonder et al., 1987]. Theoretical analyses by Bird and Kemp [1987] show that lateral variations in topography and associated isostatic variations in crustal thickness may produce lateral pressure gradients in the weak lower crust, which would induce ductile flow. They also show that, with a typical Basin and Range geotherm, periodic Moho variations with 10-km amplitude and 200-km wavelength can be destroyed in less than 1 m.y. by diffusion in the lower crust. This implies a high strain rate for the ductile deformation. Other mechanisms, such as asthenospheric flow acting on the base of the continental lithosphere, may also produce ductile flow within the midcrust and lower crust.

If directed ductile flow below the upper crust is assumed, a kinematic model for the formation of listric low-angle normal faults of regional scale can be developed purely from consideration of the orientations of principal stresses. Ductile flow in the lower crust would generate a shearing traction at the base of the brittle upper crust (Figure 1a). Such a shearing traction could, in turn, initiate low-angle extensional (detachment) shear zones cutting across the brittle upper crust (Figure 1b). Ductilely sheared midcrustal rocks (i.e., the mylonitic gneisses) would then be carried to the surface in the lower plates of such extensional detachment faults.

In Anderson's fault theory, principal stress orientations are assumed to be vertical or horizontal [Anderson, 1942]. Since ductile flow in and below the midcrust would induce shearing at the horizontal or subhorizontal base of the brittle upper crust, principal stresses at this interface could no longer be vertical and horizontal. A simple elastic model is developed in this paper to investigate the effect of basal shearing on stress distributions in the brittle upper crust. In this model I examine two classes of stress conditions which are superposed on a basal shear stress field induced by a subhorizontal basal shear traction: (1) a stress field in which the vertical gradient of the horizontal normal stress component, $\partial\sigma_{xx}/\partial y$, is constant, and (2) one in which the vertical gradient of the horizontal normal stress component, $\partial\sigma_{xx}/\partial y$, varies linearly in the horizontal direction.

In this paper I show that parallel belts of compression and extension can be simulated by considering the basal shear traction. The compressional or extensional belts can be partially or completely removed from the cross section affected by basal shear traction if a uniform tensile or compressive horizontal stress is added to the superposed stress field. Consideration of the basal shear traction may resolve the mechanical paradox of low-angle normal faults. In addition to the basal shear traction, the vertical gradient of the horizontal normal stress component is crucial in determining whether the stress field favors the formation of low-angle or high-angle normal faults. Finally, I discuss tectonic implications of the mechanical model for the formation of low-angle normal fault systems in the high Himalayas and Cenozoic extension in the North American Cordillera.

Soft-sediment listric normal growth faults (e.g., Gulf Coast), are fundamentally different from the rooted crustal-scale low-angle normal faults because they do not involve basement [Bally et al., 1981]. The mechanical origin of listric normal growth faults has been discussed by numerous workers [e.g., Crans et al., 1980; Xiao and Suppe, 1986; Bradshaw and Zoback, 1988] and is not discussed in this paper.

MECHANICAL MODEL

Figure 2a represents a simplified brittle and ideally elastic upper crust. L is the half length of the upper crust affected by basal shear traction, and H is its thickness or the depth to the brittle-ductile transition zone. Depth to brittle-ductile transition zone generally ranges from 15 to 20 km [e.g., Sibson, 1982], and the width of the Cordilleran core complexes belt varies from less than 100 km to 300 km [Coney, 1980]. Thus for the following calculations, H and L are taken to be 20 and 100 km, respectively. I assume that the state of stress during the formation of primary low-angle normal faults can be approximated by a plane stress condition. Because the upper crust is modeled as deforming elastically (following Hooke's law) before the initiation of faulting (following the Coulomb fracture criterion), the principle of superposition can be applied [Fung, 1965]. The sign convention of elasticity, used in this paper, is positive for tensile stresses (Figure 2b).

For boundary conditions the earth's surface ($y = 0$) can be taken to be traction free, i.e.,

$$\sigma_{yy}(x,0) = \tau_{xy}(x,0) = 0 \qquad (1)$$

A constant shearing traction is assumed to exist along the base of the elastic upper crust,

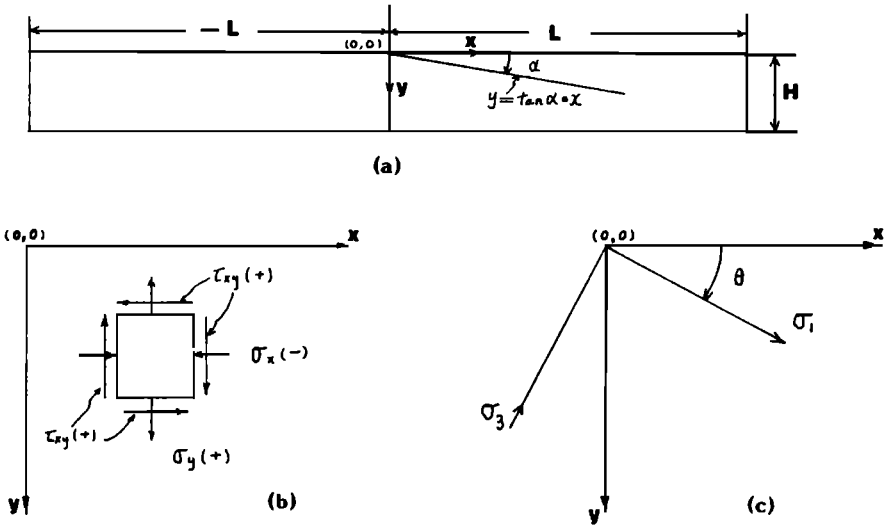

Fig. 2. (a) Geometry of an elastic-brittle upper crust. L, half length of the upper crust affected by basal shear traction. H, thickness of upper crust. (b) Sign convention for solving elastic problems. (c) θ, the angle between the maximum tensile stress σ_1 and x axis. θ is positive in the direction from x axis to y axis.

$$\tau_{xy}(x,H) = -S_0 \tag{2}$$

The negative sign preceding S_0 implies that the direction of basal shear traction acts in the negative x direction (Figure 2). The normal stress component at the base of the upper crust, $\sigma_{yy}(x,H)$, is taken to be equal to the lithostatic pressure at the depth $y = H$,

$$\sigma_{yy}(x,H) = -\rho g H \tag{3}$$

where ρ is the average density of the upper crust, and g is the acceleration of gravity. Static equilibrium of external forces applied around the boundary of the rectangular block in Figure 2a requires

$$\Sigma F_x = \Sigma F_y = \Sigma M = 0 \tag{4}$$

where ΣF_x and ΣF_y are summations of the force components in the x and y directions, and ΣM is the summation of the rotational moment.

To obtain the stress distribution in the elastic upper crust under the boundary and equilibrium conditions, I use the Airy stress function [Fung, 1965; Hafner, 1951],

$$\Phi = \frac{1}{6}k_1x^3 + \frac{1}{2}k_2x^2y + \frac{1}{2}k_3xy^2 + \frac{1}{6}k_4y^3 + \frac{1}{6}k_5xy^3 + \frac{1}{6}k_6x^3y + \frac{1}{2}k_7x^2 + \frac{1}{2}k_8y^2 \tag{5}$$

where k_i (i = 1 to 8) are arbitary constants to be determined by boundary and eqilibrium conditions. The Airy stress function satisfies the biharmonic equation

$$\nabla^4\Phi = 0 \tag{6}$$

The stress components in the x and y directions can therefore be derived from (5) [Hafner, 1951]:

$$\sigma_{xx} = \frac{\partial^2\Phi}{\partial y^2} = k_3x + k_4y + k_5xy + k_8 \tag{7}$$

$$\sigma_{yy} = \frac{\partial^2\Phi}{\partial x^2} - \rho g y = k_1x + k_2y + k_6xy + k_7 - \rho g y \tag{8}$$

$$\tau_{xy} = -\frac{\partial^2\Phi}{\partial x \partial y} = -k_2x - k_3y - \frac{1}{2}k_5y^2 - \frac{1}{2}k_6x^2 \tag{9}$$

where ρ = 2800 kg/m^3, and g = 9.8 m/s^2.

Equation (1) requires that

$$k_1 = k_2 = k_6 = k_7 = 0 \tag{10}$$

and (2) that

$$\tau_{xy}(x,H) = -k_3H - \frac{1}{2}k_5H^2 = -S_0 \tag{11}$$

Equations (7), (8), and (9) can therefore be simplified to

$$\sigma_{xx} = k_3x + k_4y + k_5xy + k_8 \tag{12}$$

$$\sigma_{yy} = -\rho g y \tag{13}$$

$$\tau_{xy} = -k_3y - \frac{1}{2}k_5y^2 \tag{14}$$

where k_3 and k_5 are defined in equation (11). The stress field specified by (12), (13), and (14) satisfies (3) and (4).

From equations (12), (13), and (14) the maximum shear stress (i.e., deviatoric stress) and the directions of the principal stresses can be determined by

$$\tau_{max} = \sqrt{\frac{1}{4}(\sigma_{xx} - \sigma_{yy})^2 + \tau_{xy}^2} \tag{15}$$

$$tan2\theta = \frac{2\tau_{xy}}{\sigma_{xx} - \sigma_{yy}} \tag{16}$$

respectively, where θ is the angle between the maximum tensile stress σ_1 and the x axis (Figure 2c). Using equations (15), (16), and by applying the Coulomb fracture criterion and the assumption that the angle of internal

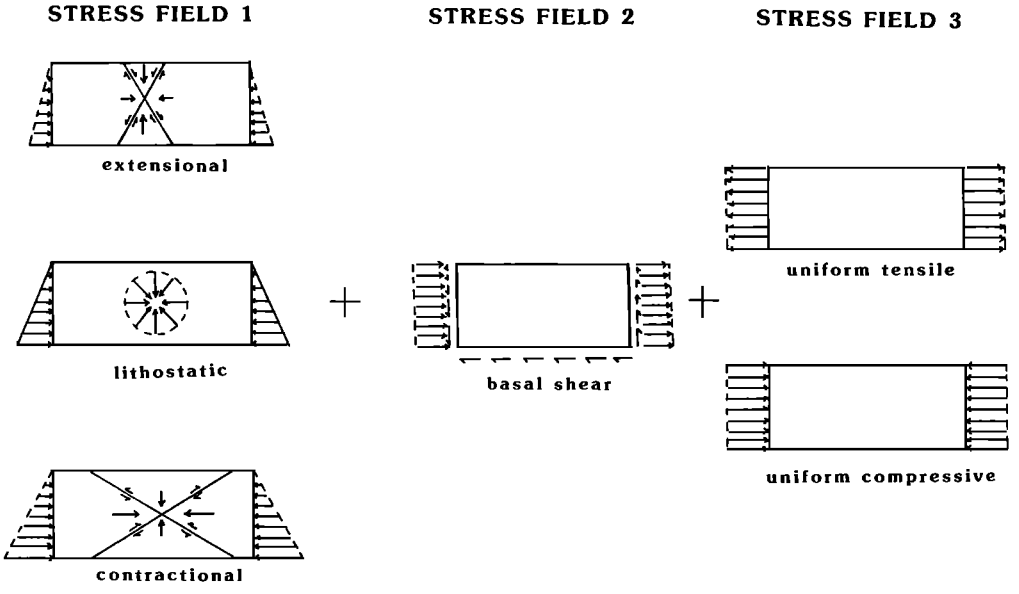

Fig. 3. Schematic diagram showing decomposition of a stress field. Arrows around the rectangular blocks show the relative magnitude of the x and y components of traction. See text for explanations.

friction is 30^0, distributions of the maximum shear stress, trajectories of the principal stresses, and predicted fault patterns for different boundary conditions were plotted by computer.

Constant Vertical Gradients of Horizontal Normal Stress Component

For a constant vertical gradient of the horizontal normal stress component, equation (12) requires that $k_5 = 0$. Now, k_3 can be determined by equation (11),

$$k_3 = S_0/H \tag{17}$$

Equations (12), (13), and (14) can be simplified to

$$\sigma_{xx} = (S_0/H)x + k_4 y + k_8 \tag{18}$$

$$\sigma_{yy} = -\rho g y \tag{19}$$

$$\tau_{xy} = -(S_0/H)y \tag{20}$$

where k_4 and k_8 are unknown.

Values of k_4 and k_8 have clear physical meanings, which can be seen by decomposing (18), (19), and (20) into three stress fields (Figure 3). The stress components in stress field 1 are

$$^1\sigma_{xx} = k_4 y \tag{21}$$

$$^1\sigma_{yy} = -\rho g y \tag{22}$$

$$^1\tau_{xy} = 0 \tag{23}$$

where $^1\sigma_{xx}$ and $^1\sigma_{yy}$ are both principal stresses because the shear stress $^1\tau_{xy} = 0$. The magnitude of the horizontal normal stress component $^1\sigma_{xx}$ depends on k_4: (1) if $k_4 = -\rho g$, stress field 1 represents a lithostatic stress field because its deviatoric stress is zero, (2) if $k_4 > -\rho g$, stress field 1 represents an extensional stress field because its horizontal deviatoric stress is extensional ($^1\sigma_{xx} > {}^1\sigma_{yy}$), and normal faults produced by such a stress field should dip about 60^0 according to Anderson [1942], and (3) if $k_4 < -\rho g$, stress field 1 represents a contractional stress field because its horizontal deviatoric stress is compressional ($^1\sigma_{xx} < {}^1\sigma_{yy}$), and faults produced by such a stress condition are contractional and dip about 30^0, according to Anderson [1942].

The stress components in stress field 2 are

$$^2\sigma_{xx} = (S_0/H)x \tag{24}$$

$$^2\sigma_{yy} = 0 \tag{25}$$

$$^2\tau_{xy} = -(S_0/H)y \tag{26}$$

Note that the basal shear traction, $^2\tau_{xy}(x, H) = -S_0$, creates a horizontal normal stress, $^2\sigma_{xx} = (S_0/H)x$, which is tensile for $x > 0$ and compressive for $x < 0$. This is a result of force balance in the horizontal direction. Stress field 2 is called here the basal shear stress field because it is induced by a shearing traction applied on the base of the elastic upper crust.

The stress components in stress field 3 are

$$^3\sigma_{xx} = k_8 \tag{27}$$

$$^3\sigma_{yy} = 0 \tag{28}$$

$$^3\tau_{xy} = 0 \tag{29}$$

Stress field 3 consists only of a constant horizontal normal stress component, $^3\sigma_{xx} = k_8$. As its stress gradients in both the x and y directions are zero, it represents a uniform tensile (for $k_8 > 0$) or compressive stress (for $k_8 < 0$).

As the three stress components in (18), (19), and (20) are linear functions of x and y, θ is constant along the line

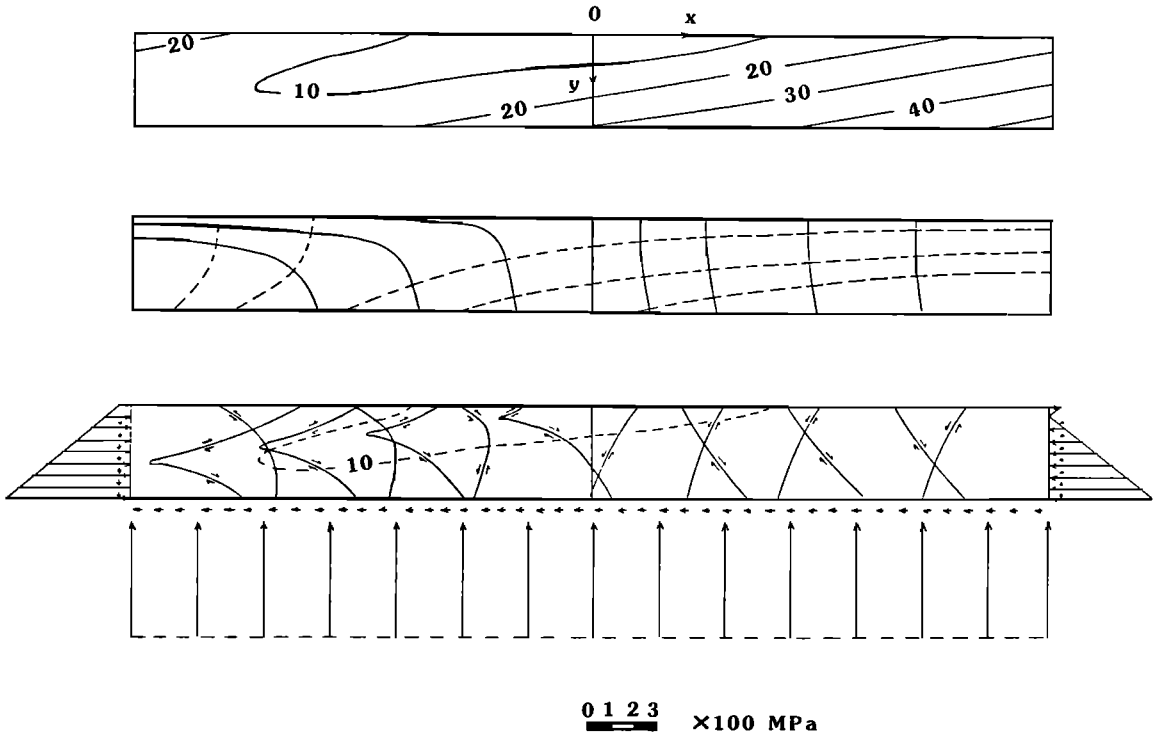

Fig. 4. Distribution of maximum shear stress (top), principal stress trajectories (middle), and predicted fault pattern (bottom) for superposition of an extensional stress field ($k_4 = -0.9\rho g$) on a basal shear stress field ($S_0 = 10$ MPa), $k_8 = 0$. Solid and dashed curves for most and least compressive stress (same in Figures 5 to 7). Arrows around the lower rectangular block show the relative magnitude of the x and y components of traction along each side of the block. Scale of the traction magnitude is shown on the bottom (same in Figures 5 to 7). Unit for stress contours is 1 MPa. The thickness of the elastic crust is $H = 20$ km, and the half length of the crust affected by the basal shear traction is $L = 100$ km (same in Figures 5 to 7). Dashed curve in fault pattern diagram is the 10-MPa contour line of τ_{max}.

$y = tan\alpha[x + k_8 H/S_0]$ (Figure 2), i.e.,

$$tan2\theta = \frac{-2(S_0/H)tan\alpha}{(S_0/H) + (k_4 + \rho g)tan\alpha} \tag{30}$$

where α is an arbitary constant and defines the slope of the line $y = tan\alpha[x + k_8 H/S_0]$. This property of the solution provides a convenient way of constructing the principal stress trajectories. In particular, if

$$(S_0/H) + (k_4 + \rho g)tan\alpha = 0 \tag{31a}$$

or

$$\alpha = tan^{-1}(\frac{-(S_0/H)}{k_4 + \rho g}) \tag{31b}$$

θ is $\pm 45^0$.

The magnitude of deviatoric stress in the Earth's lithosphere is believed to vary from 10 MPa (100 bars) to more than 100 MPa (1 kbar; [e.g., Kanamori, 1980]). The stress magnitude during the formation of quartzose mylonitic rocks of the Cordilleran core complexes has been recently investigated by Hacker et al. [1988] and Yin et al. [1988] using experimentally calibrated grain-size paleopiezometers. They show that the magnitude of flow stress (i.e., deviatoric stress or the maximum shear stress) associated with the formation of those mylonitic rocks ranges typically from 25 to 60 MPa. The results of these studies provide a basis for selecting the value of basal shear traction in the following calculations.

Figure 4 shows the distribution of the maximum shear stress, principal stress trajectories, and the predicted fault pattern for the superposition of an extensional stress field ($k_4 = -0.9\rho g > -\rho g$) on a basal-shear stress field ($S_0 = 10$ MPa), and $k_8 = 0$. The magnitude of the maximum shear stress varies from zero at the origin to more than 50 MPa at the lower right corner. The dashed curve shown in the fault pattern diagram is the 10-MPa contour line of the maximum shear stress. On the surface, $\sigma_{xx}(x, 0)$ is compressive for $x < 0$ and tensile for $x > 0$. Even though low-angle normal faults are locally present beneath a zone of contractional faults, no listric low-angle normal faults of regional extent are predicted. Predicted normal faults in the positive quadrant ($x > 0$) dip steeply and are nearly planar. Even if S_0 is as high as 50 MPa (microfiche Figure (MF) 1-4)[1], the normal faults in the positive quadrant still dip steeply. The increase of basal shear traction causes a

[1]Supplemental figures are available with entire article on microfiche. Order from American Geophysical Union, 2000 Florida Avenue, N. W., Whashington, DC 20009. Document T89001; $ 2.50. Payment must accompany order.

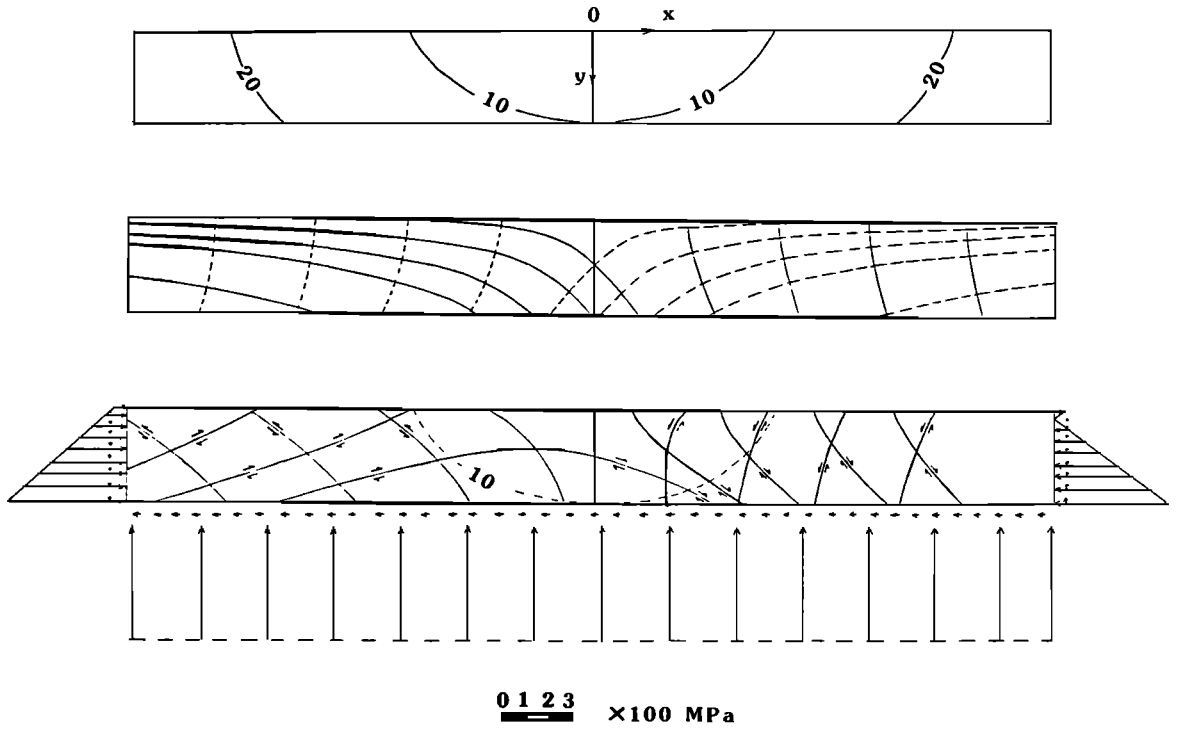

Fig. 5. Distribution of maximum shear stress, principal stress trajectories, and predicted fault pattern for superposition of a lithostatic stress field ($k_4 = -\rho g$) on a basal shear stress field ($S_0 = 10$ MPa), $k_8 = 0$. Dashed curve in fault pattern diagram is the 10-MPa contour line of τ_{max}.

significant increase of the maximum shear stress (MF 1-4). If k_8 differs from zero, then contractional faults may not occur. For example, contractional faults in Figure 4 can be completely removed from the cross section affected by basal shear stress, assuming $k_8 = 50$ MPa (MF 2-4). The normal faults predicted by such a superposed stress field are high-angle and nearly planar.

Figure 5 shows the distribution of the maximum shear stress, principal stress trajectories, and the predicted fault pattern for the superposition of a lithostatic stress field ($k_4 = -\rho g$) on a basal shear stress field ($S_0 = 10$ MPa), assuming $k_8 = 0$. On the surface, $\sigma_{xx}(x,0)$ is compressive for negative and tensile for positive x. Shear stresses predicted in this case are relatively low, ranging from zero at the origin to about 25 MPa at the lower right and lower left corners. The dashed curve shown in the fault pattern diagram in Figure 5 is the 10-MPa contour line of the maximum shear stress. From equation (30) we have

$$\theta = \frac{1}{2} tan^{-1}(-2tan\alpha) \qquad (32)$$

for $k_4 = -\rho g$. Equation (32) shows that principal stress trajectories, and the predicted fault pattern resulting from the superposition of a basal shear stress field on a lithostatic stress field, are independent of the magnitude of basal shear traction S_0. Normal faults with dips as low as 15^0 are locally present close to the line $x = 0$ (Figure 5). Although most faults are listric, none are regional low-angle faults.

Figure 6a shows the distribution of the maximum shear stress, principal stress trajectories, and the predicted fault pattern for the superposition of a contractional stress field ($k_4 = -1.1\rho g$) on a basal shear stress field ($S_0 = 10$ MPa), assuming $k_8 = 0$. On the surface, $\sigma_{xx}(x,0)$ is compressive for negative and tensile for positive x. The maximum shear stress ranges from zero at the origin to about 53 MPa in the lower left corner. As shown in Figure 6a, listric low-angle normal faults of regional extent that maintain their low-angle geometry only a few kilometers below the surface are predicted in the quadrant for positive x. Increasing basal shear traction from 10 to 50 MPa steepens the normal faults (MF 3-6). At $k_8 = 55$ MPa the origin in Figure 6a is shifted 110 km to the left (Figure 6b). This means that the superposition of a uniform tensile stress field can remove the contractional faults from the cross section affected by basal shear in Figure 6a. Note that the upper portions of most low-angle normal faults in Figure 6b lie within the region where τ_{max} is less than 10 MPa. Their lower portions close to the base of the cross section, however, lie in the region where τ_{max} is greater than 10 MPa. This result suggests that the formation of the low-angle normal faults would initiate from deep structural levels and then propagate upward, a prediction consistent with the seismological observation that most earthquakes nucleate at the base of the brittle upper crust [Sibson, 1982]. At $k_8 = -55$ MPa a uniform compressive stress is superposed, and the origin in Figure 6a is shifted 110 km to the right: the extensional faults are completely removed from the cross section (MF 4-6).

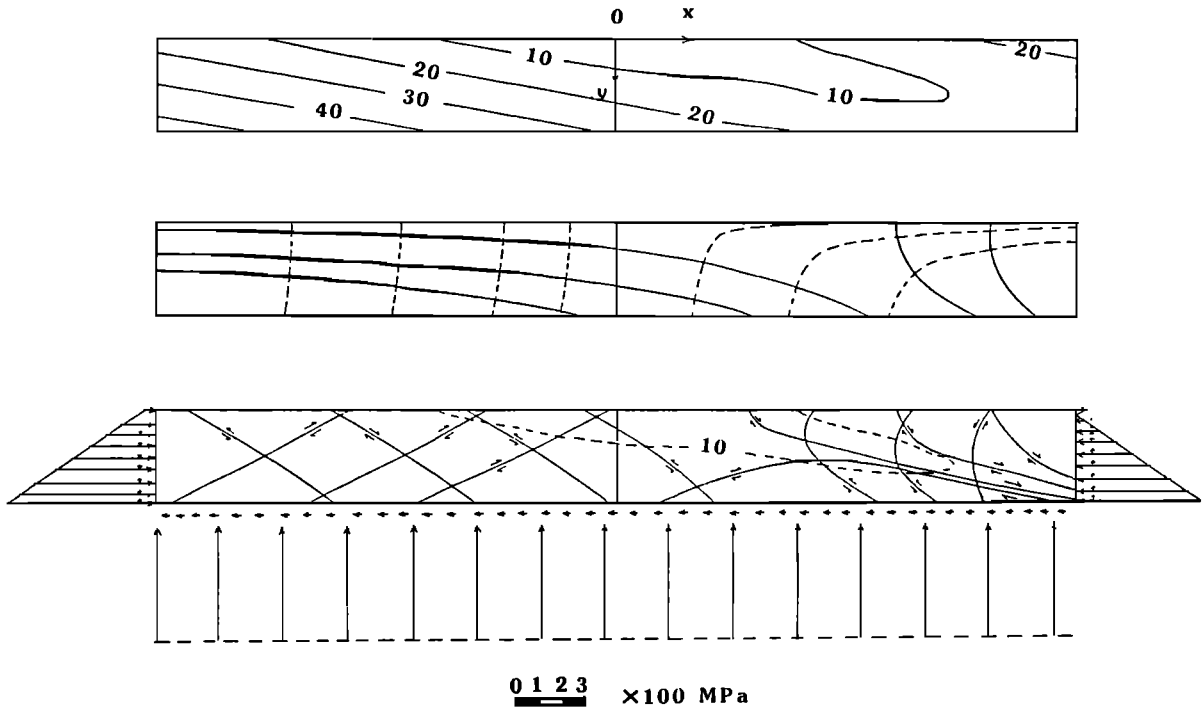

Fig. 6a. Distribution of maximum shear stress, principal stress trajectories, and predicted fault pattern for superposition of a contractional stress field ($k_4 = -1.1\rho g$) on a basal shear stress field ($S_0 = 10$ MPa), $k_8 = 0$. Dashed curve in fault pattern diagram is the 10-MPa contour line of τ_{max}.

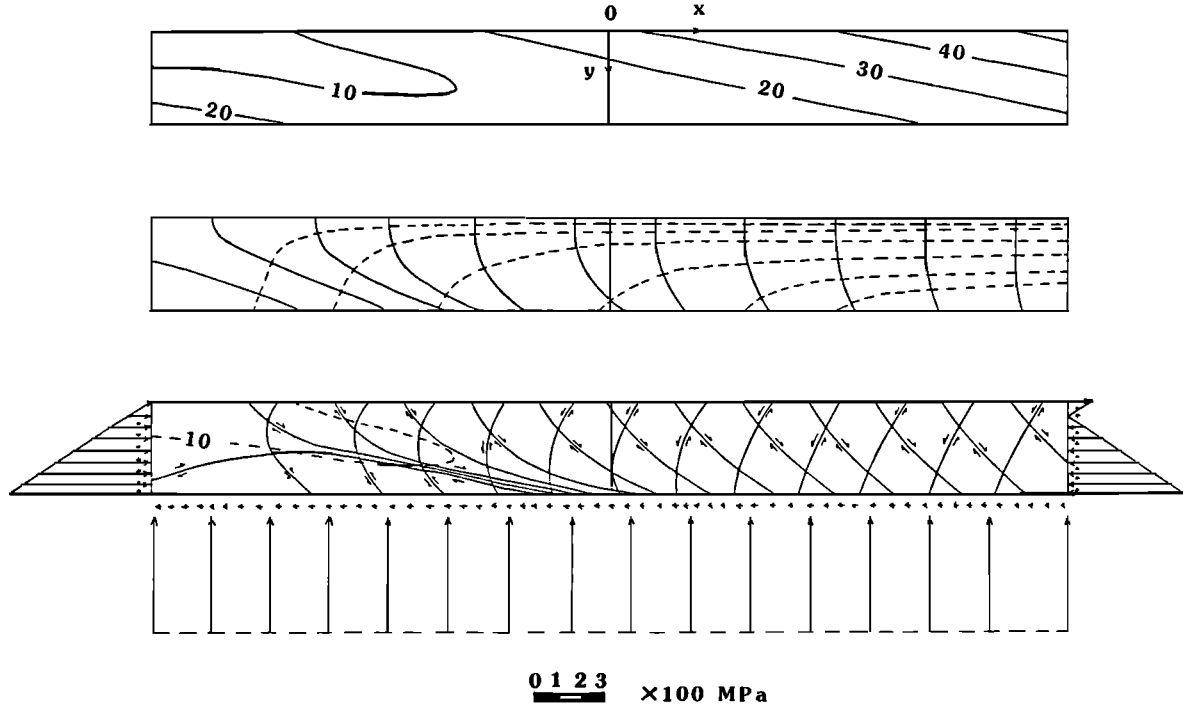

Fig. 6b. Distribution of maximum shear stress, principal stress trajectories, and predicted fault pattern for superposition of a contractional stress field ($k_4 = -1.1\rho g$) on a basal shear stress field ($S_0 = 10$ MPa) and a uniform tensile stress field ($k_8 = 55$ MPa). Dashed curve in fault pattern diagram is the 10-MPa contour line of τ_{max}.

Linear Increase/Decrease of Vertical Gradients of Horizontal Normal Stress Component in the Direction of Basal Shear Traction

The magnitude of the vertical gradient of horizontal normal stress measured in the uppermost part of the crust can vary from place to place even within the same tectonic province [e.g., McGarr and Gay, 1978]. The variations generally range from $0.5\rho g$ to $1.5\rho g$. In order to explore the effect of change in the vertical stress gradient of horizontal normal stress components on the stress distribution in the upper crust, k_5 in equation (12) is assumed not to be zero. In this case the vertical gradient of the horizontal normal stress component is a linear function of the horizontal coordinate x,

$$\frac{\partial \sigma_{xx}}{\partial y} = k_4 + k_5 x \tag{33}$$

Two conditions are considered here. First, I assume that the vertical gradient of the horizontal normal stress component, $\partial\sigma_{xx}/\partial y$, in equation (12) increases linearly in the direction of basal shear traction from $x = L$ to $x = -L$. At $x = L$ it is equal to the gradient of lithostatic pressure,

$$\frac{\partial \sigma_{xx}}{\partial y}(L, y) = k_4 + k_5 L = -\rho g \tag{34}$$

and at $x = -L$, it increases to -0.5ρg,

$$\frac{\partial \sigma_{xx}}{\partial y}(-L, y) = k_4 - k_5 L = -0.5\rho g \tag{35}$$

The boundary conditions imply that the vertical gradient of the horizontal normal stress component is greater than that of lithostatic pressure everywhere within the elastic upper crust affected by the basal shear traction except along the line $x = L$. From equation (11) we have

$$\tau_{xy}(x, H) = -k_3 H - \frac{1}{2} k_5 H^2 = -S_0 \tag{36}$$

Solving equations (34), (35), and (36), we find that

$$k_3 = (S_0/H) - \frac{1}{2} k_5 H \tag{37a}$$

$$k_4 = -0.75\rho g \tag{37b}$$

$$k_5 = -0.25\rho g/L \tag{37c}$$

Figure 7a shows the distribution of the maximum shear stress, principal stress trajectories, and the predicted fault pattern for a linear increase of the vertical gradient of the horizontal normal stress component in the direction of basal shear traction, $k_8 = 0$, and $S_0 = 10$ MPa. The maximum shear stress increases from zero at the origin to

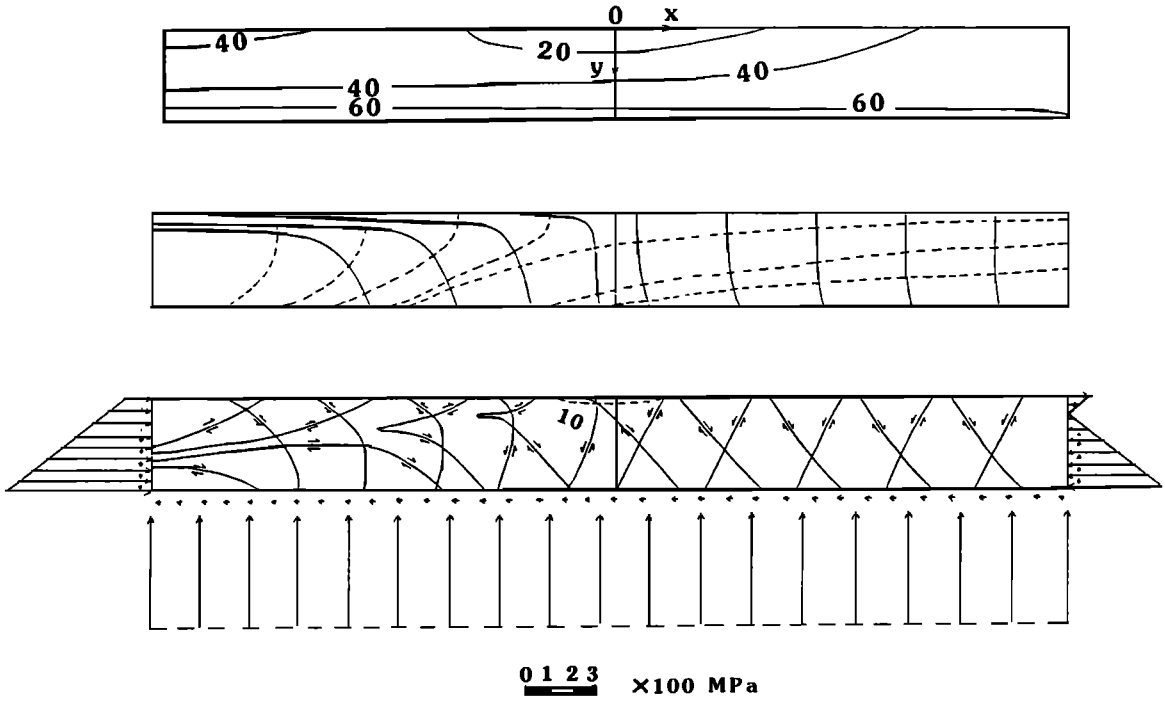

Fig. 7a. Distribution of maximum shear stress, principal stress trajectories, and predicted fault pattern for a superposed stress field in which the vertical gradient of horizontal normal stress component increases linearly in the direction of basal shearing, $S_0 = 10$ MPa, $k_3 = (S_0/H) - 0.5k_5 H$, $k_4 = -0.75\rho g$, $k_5 = -0.25\rho g/L$, and $k_8 = 0$. Dashed curve in fault pattern diagram is the 10-MPa contour line of τ_{max}.

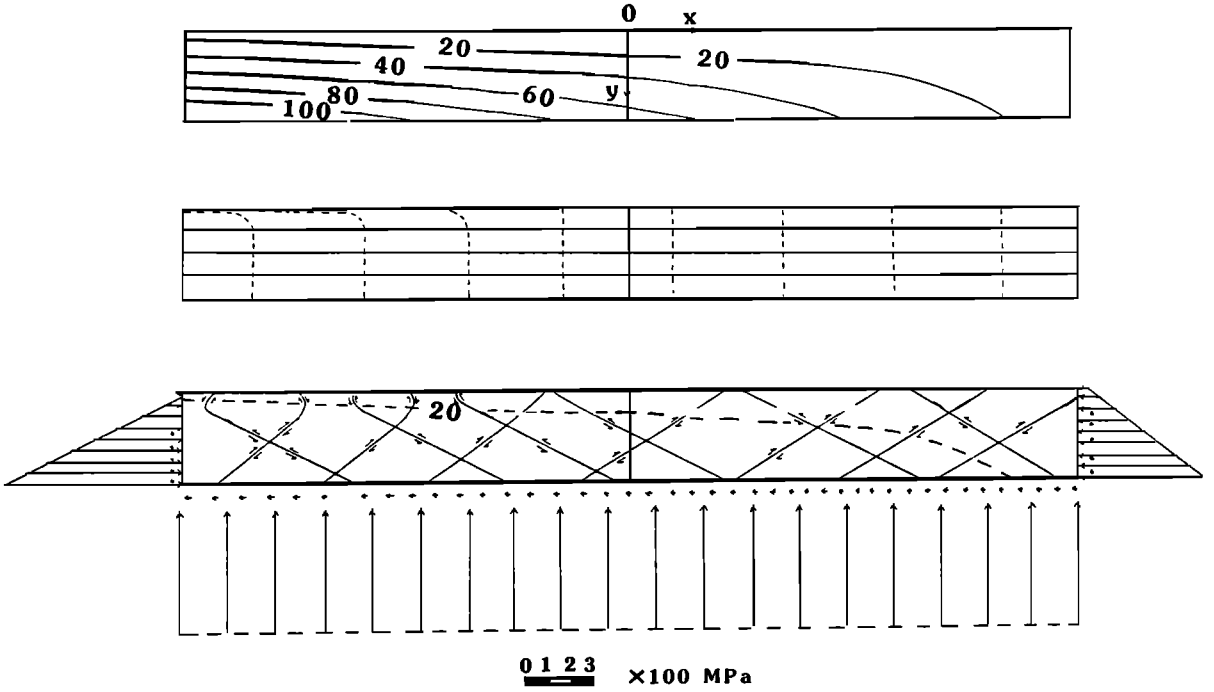

Fig. 7b. Distribution of maximum shear stress, principal stress trajectories, and predicted fault pattern for a superposed stress field in which the vertical gradient of horizontal normal stress component decreases linearly in the direction of basal shearing, $S_0 = 10$ MPa, $k_3 = (S_0/H) - 0.5k_5H$, $k_4 = -1.25\rho g$, $k_5 = 0.25\rho g/L$, and $k_8 = 0$. Dashed curve in fault pattern diagram is the 20-MPa contour line of τ_{max}.

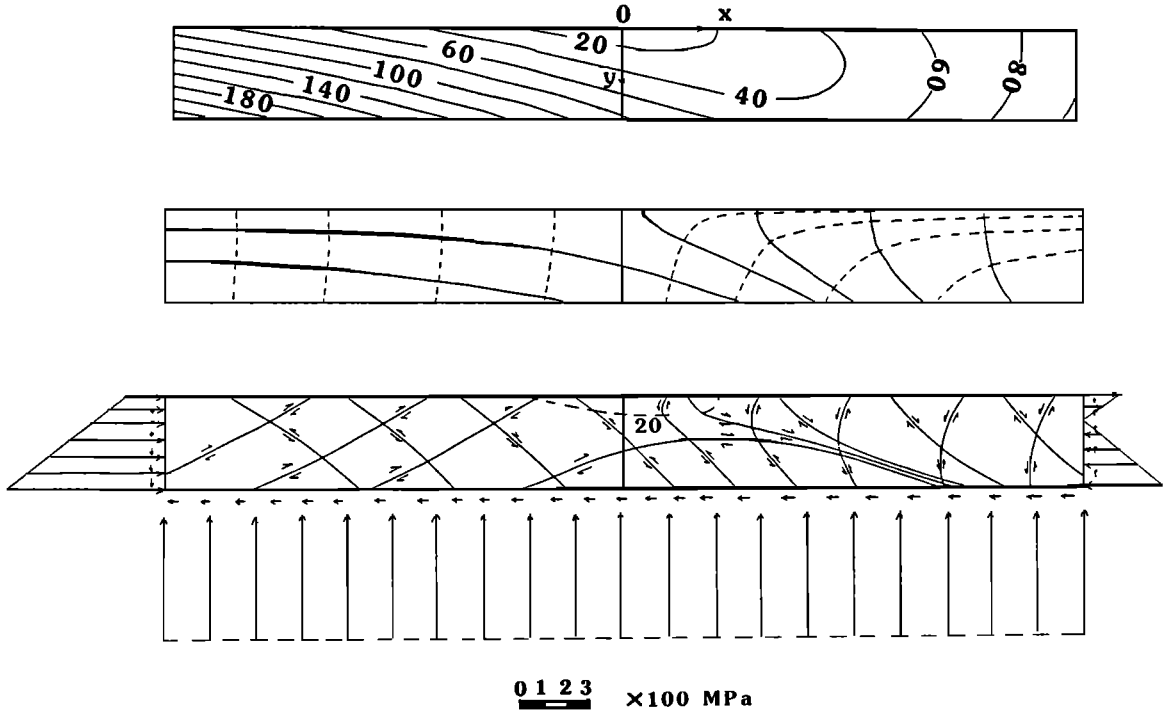

Fig. 7c. Distribution of maximum shear stress, principal stress trajectories, and predicted fault patterns for a superposed stress field in which the vertical gradient of horizontal normal stress component decreases linearly in the direction of basal shearing, $S_0 = 50$ MPa, $k_3 = (S_0/H) - 0.5k_5H$, $k_4 = -1.25\rho g$, $k_5 = 0.25\rho g/L$, and $k_8 = 0$. Dashed curve in fault pattern diagram is the 20-MPa contour line of τ_{max}.

more than 60 MPa in the lowermost part of Figure 7a. On the surface, $\sigma_{xx}(x,0)$ is tensile for positive and compressive for negative x. Such parallel belts of extension and compression are induced by the basal shear traction $\tau_{xy}(x,H) = -k_3H - \frac{1}{2}k_5H^2 = -S_0$ as a result of force balance in the horizontal direction. Consequently, contractional faults that reach the surface are predicted in the quadrant for negative x and extensional faults that reach the surface in the quadrant for positive x. Although low-angle normal faults are locally predicted beneath thrust faults in the negative quadrant, none are listric low-angle normal faults of regional extent. Normal faults in the region $x >> 0$ dip steeply and are nearly planar. The dashed curve in the diagram of the predicted fault pattern is the 10-MPa contour line for the maximum shear stress. Increasing basal shear traction from 10 to 50 MPa slightly reduces the dip angle of these normal faults but increases the maximum shear stress significantly (MF 5-7).

For a linear decrease of the vertical gradient of the horizontal normal stress component in the direction of basal shear traction, I assume that at $x = L$

$$\frac{\partial \sigma_{xx}}{\partial y}(L,y) = k_4 + k_5 L = -\rho g \tag{38}$$

where $-\rho g$ is the gradient of lithostatic pressure, and at $x = -L$, the stress gradient decreases to -1.5ρg,

$$\frac{\partial \sigma_x}{\partial y}(-L,y) = k_4 - k_5 L = -1.5\rho g \tag{39}$$

These boundary conditions imply that the vertical gradient of the horizontal normal stress component is less than that of lithostatic pressure everywhere in the elastic upper crust affected by the basal shear traction, except along the line $x = L$. This may represent a setting near a convergent plate boundary, where the vertical stress gradient of the horizontal normal stress component is greatest near the contact of the two convergent plates ($x < -L$) and decreases away from it. It reaches the gradient of lithostatic pressure at a distance sufficiently far away from the contact ($x \geq L$). From equation (11) we have

$$\tau_{xy}(x,H) = -k_3H - \frac{1}{2}k_5H^2 = -S_0 \tag{40}$$

Solving equations (22), (23), and (24), we find that

$$k_3 = (S_0/H) - \frac{1}{2}k_5H \tag{41a}$$

$$k_4 = -1.25\rho g \tag{41b}$$

$$k_5 = 0.25\rho g/L \tag{41c}$$

Figure 7b shows the distribution of the maximum shear stress, principal stress trajectories, and the predicted fault pattern for a linear decrease of the vertical gradient of the horizontal normal stress component in the direction of the basal shear traction, $k_8 = 0$, and S_0=10 MPa. The magnitude of the maximum shear stress predicted by this stress condition increases downward from zero at the origin to about 100 MPa at the lower left part of the section. On the surface, $\sigma_{xx}(x,0)$ is compressive for positive and tensile for negative x. As a consequence, extensional faults that reach the surface are predicted for the negative quadrant, whereas contractional faults that reach the surface are predicted for the positive quadrant. Extensional faults are only present in the uppermost part of the negative quadrant and none are listric low-angle normal faults of regional extent. Increasing basal shear traction from 10 to 50 MPa switches the sign of σ_{xx} on the surface to $\sigma_{xx}(x,0) > 0$ (tensile) for $x > 0$ and $\sigma_{xx}(x,0) < 0$ (compressive) for $x < 0$ (Figure 7c). This indicates that the polarity of extensional and contractional belts depends not only on the direction of basal shear traction but also on its magnitude if $\partial\sigma_{xx}/\partial y$ varies horizontally. Furthermore, the increase of basal shear traction can cause regional low-angle normal faults which intersect the surface in a zone 30-40 km wide in the positive quadrant (Figure 7c). Although regional low-angle normal faults are predicted in both Figures 6a and 7c, the corresponding distributions of the maximum shear stress are quite different. In Figure 6a, most predicted low-angle normal faults are within the region where the maximum shear stress is less than 10 MPa. In contrast, most predicted regional low-angle normal faults are present in the region where the maximum shear stress is greater than 20 MPa.

Under the stress conditions represented by Figures 7a, MF 5-7, 7b, and 7c, k_8 is assumed to be zero. If k_8 differs from zero, the patterns of principal stress trajectories and predicted faults in Figures 7a, MF 5-7, 7b, and 7c do not change appreciably but shift to the right for positive or to the left for negative k_8. This is shown in MF 6-7 for a stress condition identical with that represented in Figure 7c, except that $k_8 = 50$ MPa. Superposition of this uniform tensile stress field, k_8=50 MPa, causes the origin in Figure 7c to shift about 27 km to the left and to remove the contractional faults in the region $x << 0$ of Figure 7c from the cross section affected by basal shear traction. A tensile stress of about 185 MPa is required to remove all contractional faults in Figure 7c that reach the surface.

TECTONIC IMPLICATIONS

Low-angle Normal Faults in the High Himalayas

E-W striking, gently northerly dipping normal faults in the high Himalayas and southern Tibet were recently recognized by Burg et al. [1984]. These faults extend for at least 600 km along strike. Burchfiel and Royden [1985] interpreted them as probably late (?) Miocene extensional features, on which movement was synchronous with the development of compressional belts to the south and the north. A two-mica granite which cuts an E-W down-to-the-north normal fault on the north face of Mount Everest has been dated by U-Pb and $^{40}Ar/^{39}Ar$ methods by Copeland et al. (1987) as 22 m.y. ago, indicating that motion along the northerly dipping normal fault systems occurred as early as 22 m.y. ago. On the basis of an elastic model which simulates stress distributions for the superpostion of a compressional horizontal stress with a topographic load, Burchfiel and Royden [1985] postulated that the low-angle normal faults in southern Tibet and the high Himalayas are direct results of gravity acting on areas of high topography that formed in response to a thickening of the crustal root. However, the stress trajectories produced by their model predict that the maximum compressive stress is inclined southward from steep to shallow angles [Burchfiel and Royden, 1985; Figure 4]. The corresponding listric low-angle normal faults predicted by such a stress condition should also dip to the south. This, however, contradicts the fact that the low-angle normal faults in the high Himalayas are rooted to the north into

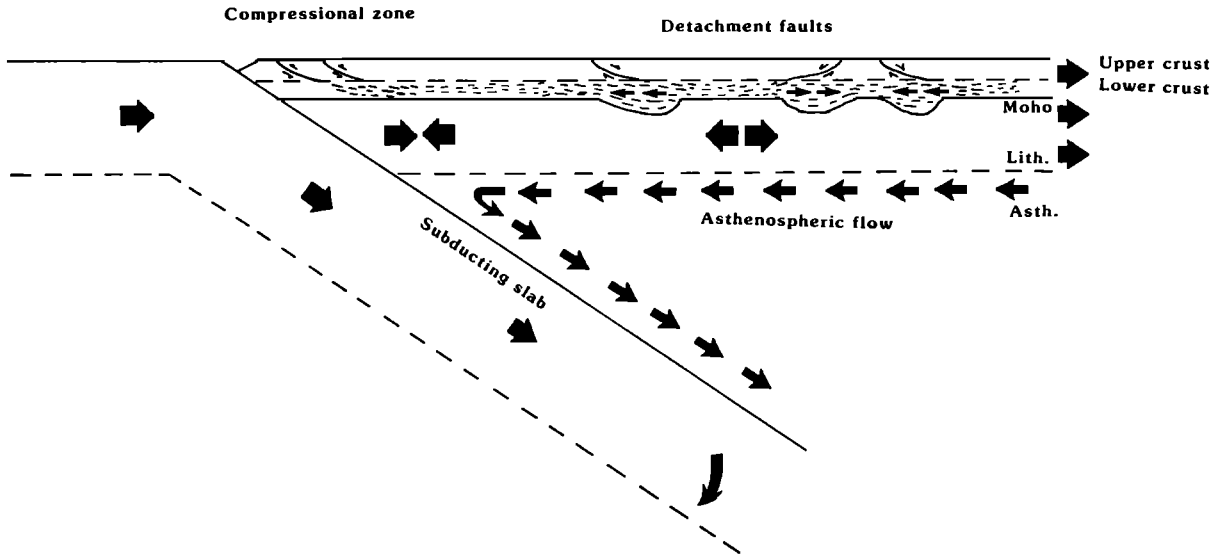

Fig. 8. Diagrammatic cross section showing possible boundary forces responsible for the formation of rooted low-angle normal faults in western North America during the mid-Tertiary.

the mountain belt. The proposed kinematic model (Figure 2) and the results of my calculations may help to resolve this problem. As pressure varies with surface elevation, a lateral pressure gradient is required in the weak lower crust [Bird and Kemp, 1987]. Such a pressure gradient in the lower crust would cause ductile flow toward the low-elevation region. In the Himalayan region this would require a south-directed ductile flow in the weak lower crust. In the kinematic model proposed here, listric low-angle normal faults of regional extent dipping to the north in the direction opposite to the basal shear traction may be produced by either of the superposed stress fields. These are (1) the superposition of a basal shear stress field on a contractional stress field (Figure 6a), or (2) the superposition of a stress field in which the vertical gradient of horizontal normal stress component decreases linearly in the direction of basal shearing on a basal shear stress field with a strong basal shear traction (Figure 7c). Both superposed stress fields can be caused by plate convergence or subduction. These simulated stress conditions not only predict the geometry and dip direction of listric low-angle normal faults but also the presence of contemporaneous E-W striking thrust belts and low-angle normal faults in the high Himalayas [Burchfiel and Royden, 1985].

Cenozoic Extension in Western North America

Late Cenozoic extensional tectonism in the North American Cordillera, as expressed in the Basin and Range Province, has been well documented [e.g., Stewart, 1978]. An earlier period of mid-Tertiary Cordilleran extensional tectonics has only recently been recognized [Armstrong, 1972; Crittenden et al., 1980]. The mid-Tertiary extensional terranes (the Cordilleran metamorphic core complexes; [Coney, 1980]), are characterized by major, gently dipping detachment faults that separate a brittlely distended upper plate from a lower plate consisting mostly of plutonic and metamorphic rocks. The tectonic origin of the Cordilleran core complexes is the subject of controversy. Coney [1980] and Dickinson [1981], among others, proposed that the formation of the core complexes was related to interactions between the North American plate and Pacific plates. They believed that changes in plate kinematics during Oligocene-Miocene was the main cause for initiation of the mid-Tertiary extension in western North America.

Observing that the mid-Tertiary inception of the Cordilleran core complexes was associated with a westward retrograde sweep of massive ignimbrite outbursts [Coney and Reynolds, 1977], and that the locus of core complex extension corresponds to that of Mesozoic crustal thickening, Coney and Harms [1984], and Coney [1987] proposed that core complex extension took place only when a sharp pulse of magmatism swept across the thickened welt. This pulse of magmatism lowered the crustal viscosity and allowed the gravitationally unstable crustal welt to spread laterally. Sonder et al. [1987], on the basis of a theoretical analysis, proposed a similar model in which the thick continental lithosphere formed during the Sevier and Laramide orogenies was the cause for the Cenozoic extension in western North America because it was gravitationally unstable and would tend to spread under its own weight.

The mechanical model developed in this paper allows one to test, quantitatively, tectonic hypotheses for the origin of the Cordilleran metamorphic core complexes. Assuming that the upper crust was deformed elastically during extension and that the gravitational spreading of the weak lower crust produced a constant shear traction on the base of the upper crust, calculations show that the gravitational spreading itself is insufficient to produce rooted low-angle detachment faults (Figure 5). External forces seem required to produce appropriate stress gradients and additional tensile stress (Figures 6a, 6b, 7c, and MF 6-7). This suggests that forces generated inside the North American plate may not be the only factors to have initiated core complex extension.

Figure 8 shows possible boundary conditions for the formation of Cordilleran core complexes. The recon-

structed plate tectonic setting of mid-Tertiary extension suggests that subduction of the Farallon plate along the western margin of North America continued during the mid-Tertiary [e.g., Coney, 1980, 1987]. A contractional stress field related to this plate subduction caused the development of compressional structures along the western margin of the North American plate. The location of core complexes was controlled by thickened crustal welts [Coney and Harms, 1984]; their gravitational spreading caused ductile flow and a shear traction on the base of the upper crust, which in turn produced a basal shear stress field. The inclination of regional low-angle detachment faults in the North American Cordillera [Wust, 1986] was controlled by the flow direction in and below the midcrust. West-directed asthenospheric flow, which may have been initiated by the collapse and/or steepening of the subducting plate [Coney and Reynolds, 1977], caused a uniform tensile stress field in the continental interior and synchronous compression along the western margin of the North American plate [e.g., Wernicke et al., 1987]. The stress field induced in the lithosphere by asthenospheric flow resembles the basal shear stress field generated by gravitational spreading (see Figure 3), except that it controls deformation of the continental lithosphere on a larger scale.

A major change in structural style from dominant listric low-angle normal to high-angle block faulting in western North America during the beginning of the Late Tertiary has long been noted [e.g., Coney, 1980; Zoback et al., 1981], although exceptions do exist locally [e.g., Burchfiel et al., 1987]. This change has been attributed to interactions between the North American plate and Pacific plates [Coney, 1980; Dickinson, 1981; Zoback et al., 1981; Armstrong, 1982]. As shown in MF 2-4, the superposition of an extensional stress field (tensile horizontal deviatoric stress) on a basal shear stress field and a uniform tensile stress field can produce high-angle normal faults. In contrast, the superposition of either a contractional stress field (compressional horizontal deviatoric stress) or a stress field with $\partial\sigma_{xx}/\partial y$ decreasing linearly in the direction of basal shearing from $-\rho g$ to $-1.5\rho g$ on a basal shear stress field and a uniform tensile stress field can simulate the geometry of rooted low-angle detachment faults (Figures 6b, MF 6-7). It is likely that the aforementioned change in structural style corresponds to the termination of a contractional stress field induced by plate subduction and the beginning of an extensional stress field (extensional horizontal deviatoric stress) caused by a diffuse transform interaction between the North American and Pacific plates [Atwater, 1970; Ingersoll, 1982].

It is important to point out that the model presented here predicts only the initiation of faulting, because the Coulomb fracture criterion is assumed. It does not, however, preclude possible reactivation of mid-Tertiary low-angle normal faults and older thrust faults during the late Cenozoic Basin and Range extension, which has produced most of the present topography. It is also important to note that this paper deals with an inverse problem. Because of this, states of stress simulated in an elastic upper crust in this study are only a few of the many under which listric low-angle normal faults may occur.

CONCLUSIONS

Consideration of a basal shear stress field, induced by a shearing traction acting on the base of the upper crust, helps to resolve the mechanical paradox of rooted low-angle detachment faults. Theoretical stress analyses of an elastic upper crust suggest that listric normal faults of regional extent, with shallow dips at the time of their inception, can be simulated by superposition of a contractional stress field on a basal shear stress field. This superposed stress field also predicts parallel belts of extension and compression in the cross section affected by basal shear traction. These results not only explain the occurrence of low-angle normal faults in the high Himalayas but also their dip direction, assuming that the weak lower crust is capable of flowing under the pressure gradient induced by lateral variation of elevation and the associated isostatic variations in crustal thickness. If the vertical gradient of the horizontal normal stress component is constant, the polarity of the predicted compressional and extensional belts only depends on the direction of the basal shear traction. If it varies linearly in the horizontal direction, however, the polarity depends not only on the basal shear direction but on the shear traction magnitude as well. Calculations suggest that a constant basal shear traction induced by gravitational spreading of the weak lower crust itself is insufficient to produce stress conditions compatible with core complex extension in western North America. External forces along plate boundaries seem required to provide appropriate stress gradients and additional tensile stress.

Acknowledgments. Unpublished manuscripts by Gordon Lister and Greg Davis have helped me to develop this mechanical model. Stimulating discussions on the origin of low-angle normal faults with Greg Davis, Jay Jackson, Clem Chase, and Terry Wallace during the early stage of this research have been extremely helpful. Critical reviews from Greg Davis, C.Y. Wang, Ray Ingersoll, Gerhard Oertel, E.R. Rutter, Peter Bird, John Christie, Sue Orrell, Sandy Steacy, and X.F. Chen improved the original manuscript and are greatly appreciated. I would like to thank Gerhard Oertel and Dave Diamond for their helpful comments and careful reviews of the manuscript. I am particularly in debt to the *Tectonics* reviewers, H. Jay Melosh and Craig Jones, who pointed out and helped me to correct many errors in the early version of this paper. I am grateful to Helen Qian who wrote computer programs for plotting the results. This research was partially supported by NSF grant EAR-09695 to J.L. Anderson and G.A. Davis.

REFERENCES

Allmendinger, R.W., J.W. Sharp, D. Von Tish, L. Serpa, L. Brown, S. Kaufman, and J. Oliver, Cenozoic and Mesozoic structure of the eastern Basin and Range from COCORP seismic reflection data, *Geology, 11*, 532-536, 1983.

Anderson, E.M., *The Dynamics of Faulting and Dyke Formation with Application to Britain*, 191 pp. Oliver and Boyd, Edinburgh, Scotland, 1942.

Anderson, J. L., Core complexes of Mojave-Sonora Desert: Conditions of plutonism, mylonitization, and decompression, in *Metamorphic and Tectonic Evolution of the Western Cordillera, Conterminous United States, Rubey* vol. 7, edited by W.G. Ernst, pp. 502-537, Prentice-Hall, Englewood Cliffs, N. J., 1988.

Armstrong, R.L., Low-angle (denudational) faults, hinterland of the Sevier orogenic belt, eastern Nevada and western Utah, *Geol. Soc. Am. Bull., 83*, 1729-1754, 1972.

Armstrong, R.L., Cordilleran metamorphic core complexes from Arizona to southern Canada, *Annu. Rev. Earth Planet. Sci., 10*, 129-154, 1982.

Atwater, T., Implications of plate tectonics for the Cenozoic tectonic evolution of western North America, *Geol. Soc. Am. Bull., 81*, 3513-3536, 1970.

Bally, A.W., D. Bernoulli, G.A. Davis, and L. Montadert, Listric normal faults, Proceedings 26^{th} International Geological Congress, Geology of Continental Margins Symposium, *Oceanol. Acta, 4*, 87-101. 1981.

Bird, P., and D. Kemp, Nonlinear diffusion of crustal thickness and topography, *Eos Trans. AGU, 68*, 1465, 1987.

Bradshaw, G.A., and M.D. Zoback, Listric normal faulting, stress refraction, and the state of stress in the Gulf Coast basin, *Geology, 16*, 271-274, 1988.

Burchfiel, B.C., and L.H. Royden, North-south extension within the convergent Himalayan region, *Geology, 13*, 679-682, 1985.

Burchfiel, B.C., K.V. Hodges, and L.H. Royden, Geology of Panamint Valley-Saline Valley pull-apart system, California: Palinspastic evidence for low-angle geometry of a Neogene range-bounding fault, *J. Geophys. Res., 92*, 10422-10426, 1987.

Burg, J.P., M. Brunel, D. Gapais, G.M. Chen, and G.H. Liu, Deformation of leucogranites of the crystalline main central thrust sheet in southern Tibet (China), *J. Struct. Geol., 6*, 535-542, 1984.

Chen, W.P., and P. Molnar, Focal depth of intracontinental and intraplate earthquakes and their implications for the thermal and mechanical properties of the lithosphere, *J. Geophys. Res., 85*, 4183-4214, 1983.

Coney, P.J., Cordilleran metamorphic core complexes: An overview, in *Cordilleran Core Complexes*, Mem. 153, edited by M. L. Crittenden, Jr., P.J. Coney, and G.H. Davis, pp. 7-34, *Geological Society of America*, Boulder, Colo., 1980.

Coney, P.J., The regional tectonic setting and possible causes of Cenozoic extension in the North American Cordillera, in *Continental Extensional Tectonics, Spec. Publ. 28*, edited by M.P. Coward, J.F. Dewey, and P.L. Hancock, *Geological Society of London*, pp. 177-186, 1987.

Coney, P.J., and T.W. Harms, Cordilleran metamorphic core complexes: Cenozoic extensional relics of Mesozoic compression, *Geology, 12*, 550-554, 1984.

Coney P.J., and S.J. Reynolds, Cordilleran Benioff Zones: *Nature, 270*, 403-406, 1977.

Copeland, P., T.M. Harrison, R. Parish, B.C. Burchfiel, K. Hodges, and W.S.F. Kidd, Constraints on the age of normal faulting, north face of Mt. Everest: Implications for Oligo-Miocene uplift, *Eos Trans. AGU, 68*, 1444, 1987.

Crans, W., G. Mandel, and J. Haremboure, On the theory of growth faulting, *J. Pet. Geol., 2*, 343-382, 1980.

Crittenden, M.D., Jr., P.J. Coney, and G.H. Davis (eds.), *Cordilleran Core Complexes, Mem. 153*, 409 pp., *Geological Society of America*, Boulder, Colo., 1980.

Davis, G.A., Rapid upward transport of mid-crustal mylonitic gneisses in the footwall of a Miocene detachment fault, Whipple Mountains, southeastern California, *Geol. Rundsch., 77*, 191-209, 1988.

Davis, G.A., and G.S. Lister, Detachment faulting in continental extension: Perspective from the southwestern U.S. Cordillera, *Spec. Pap. Geol. Soc. Am. 218*, 133-159, 1988.

Davis, G.A., J.L. Anderson, E.G. Frost, and T.J. Shackelford, Mylonitization and detachment faulting in the Whipple-Buckskin-Rawhide Mountains terrane, southeastern California and western Arizona, in *Cordilleran Core Complexes, Mem. 153*, edited by M.D. Crittenden, Jr., P.J. Coney, and G.H. Davis, pp. 79-129, *Geological Society of America*, Boulder, Colo., 1980.

Davis, G.A., G.S. Lister, and S.J. Reynolds, Structural evolution of the Whipple and South Mountains shear zones, southwestern United States, *Geology, 14*, 7-10, 1986.

Dickinson, W.R., Plate tectonic evolution of the southern Cordillera, Relations of Tectonics to Ore Deposits in the Southern Cordillera, edited by W.R. Dickinson, and W.D. Payne, *Ariz. Geol. Soc. Dig., 14*, 113-135, 1981.

Frost, E.G., and D.L. Martin (eds.), *Mesozoic-Cenozoic tectonic evolution of the Colorado River region, California, Arizona, and Nevada*, 608 pp., Cordilleran Publishers, San Diego, Calif., 1982.

Frost, E.G., and D. A. Okaya, Regional extent of mid-crustal mylonitic rocks in Arizona and So. California from seismic reflection profiles: distributed simple shear during crustal extension, *Geol. Soc. Am. Abstr. Programs, 19*, 669-670, 1987.

Fung, Y.C., *Foundations of Solid Mechanics*, 593 pp., Chapman and Hall, London, 1965.

Green, A., and B. Wernicke, Possible large-magnitude Neogene extension on the southern Peruvian Altiplano: Implications for the dynamics of mountain building, *Eos Trans. AGU, 67*, 1241, 1986.

Hacker, B.R., A. Yin, and J.M. Christie, Stress magnitude during the development of core complexes, *Geol. Soc. Am. Abstr. Programs, 20*, A139, 1988.

Hafner, W., Stress distributions and faulting, *Geol. Soc. Am. Bull., 62*, 373-398, 1951.

Ingersoll, R.V., Triple-junction instability as cause for late Cenozoic extension and fragmentation of the western United States, *Geology, 10*, 621-625, 1982.

John, B.E., Geometry and evolution of a mid-crustal extensional fault system: Chemehuevi Mountains, southeastern California, in *Continental extensional tectonics, Spec. Publ. 28*, edited by M.P. Coward, J.F. Dewey, and P.L. Hancock, eds., pp. 313-335, *Geological Society of London*, 1987.

Kanamori, H., The state of stress in the Earth's lithosphere, in *Physics of the Earth's Interior, Enrico Fermi Vol.*, edited by A.M. Dziemonski, and E. Boschi, pp. 531-554, North-Holland, New York, 1980.

McGarr, A., and N.C. Gay, State of stress in the Earth's crust, *Annu. Rev. Earth Planet. Sci., 6*, 405-436, 1978.

Sibson, R.H., Fault zone models, heat flow, and depth distribution of earthquakes in the continental crust of the United States, *Bull. Seis. Soc. Am., 72*, 151-161, 1982.

Sonder, L.J., P.C. England, B.P. Wernicke, and R.L. Christiansen, A physical model for Cenozoic extension of western North America, in *Continental Extensional Tectonics, Spec. Publ. 28*, edited by M.P. Coward, J.F. Dewey, and P.L. Hancock, pp. 187-201, *Geological Society of London*, 1987.

Stewart, J.H., Basin and Range structure in western North America: A review, in *Cenozoic Tectonics and Regional Geophysics of the Western Cordillera, Mem. 152*, edited by R.B. Smith and G.L. Eaton, pp. 1-31, *Geological Society of America*, Boulder, Colo., 1978.

Wernicke, B., Low-angle normal faults in the Basin and Range Province–Nappe tectonics in an extending orogen, *Nature, 291*, 645-648, 1981.

Wernicke, B., Uniform-sense normal shear of the continental lithosphere, *Can. J. Earth Sci., 22*, 108-125, 1985.

Wernicke, B., J.D. Walker, and M.S. Beaufait, Structural discordance between Neogene detachments and frontal

Sevier thrusts, central Mormon Mountains, southern Nevada, *Tectonics, 4*, 213-246, 1985.

Wernicke, B.P., R.L. Christiansen, P.C. England, and L.J. Sonder, Tectonomagmatic evolution of Cenozoic extension in the North American Cordillera, in *Continental Extensional Tectonics, Spec. Publ. 28*, edited by M.P. Coward, J.F. Dewey, and P.L. Hancock, pp. 203-221, *Geological Society of London*, 1987.

Wright, J.E., J.L. Anderson, and G.A. Davis, Timing and decompression in a metamorphic core complex, Whipple Mountains, Ca., *Geol. Soc. Am. Abstr. Programs, 18*, 201, 1986.

Wust, S.L., Regional correlation of extensional directions in Cordilleran metamorphic complexes, *Geology, 14*, 828-830, 1986.

Xiao, H.B., and J. Suppe, 1986. Role of compaction in the listric shape of growth faults, *Geol. Soc. Am. Abstr. Programs, 18*, 796, 1986.

Yin, A., B.R. Hacker, and J.M. Christie, Stress magnitude during the formation of mylonitic rocks in the Ruby Mountains and Snake Ranges, *Eos Trans. AGU, 69*, 1462-1463, 1988.

Zoback, M.L., R.E. Anderson, and G.A. Thompson, Cainozoic evolution of the state of stress and style of tectonism of the Basin and Range Province of the western United States, *Philos. Trans. R. Soc. London Ser. A, 300*, 189-216, 1981.

A. Yin, Department of Earth and Space Sciences, University of California, Los Angeles, CA 90024-1567.

(Received February 10, 1988;
revised January 30, 1989;
accepted February 15, 1989)